Supplemental Data

Tricellulin is essential for associating bicellular and tricellular tight junctions and for survival of cochlear hair cells

Gowri Nayak,[1] Sue I. Lee,[2] Rizwan Yousaf,[1] Stephanie Edelmann,[3] Claire Trincot,[1] Christina M. Van Itallie,[4] Ghanshyam P. Sinha,[3] Maria Rafeeq,[5] Sherri M. Jones,[6] Inna A. Belyantseva,[2] James M. Anderson,[4] Andrew Forge,[7] Gregory I. Frolenkov,[3] Saima Riazuddin,[1]

[1]Laboratory of Molecular Genetics, Division of Pediatric Otolaryngology Head & Neck Surgery, Cincinnati Children's Hospital Research Foundation, and the Department of Otolaryngology, College of Medicine, University of Cincinnati, Cincinnati, Ohio, USA. [2]Section on Human Genetics, Laboratory of Molecular Genetics, National Institute on Deafness and Other Communication Disorders, National Institutes of Health, Rockville, Maryland, USA. [3]Department of Physiology, University of Kentucky, Lexington, Kentucky, USA.[4] National Heart, Lung, and Blood Institute, National Institutes of Health, Bethesda, Maryland, USA.[5]National Center of Excellence in Molecular Biology, University of the Punjab, Lahore, Pakistan. [6]Department of Special Education and Communication Disorders, University of Nebraska, Omaha, Nebraska, USA.[7]Centre for Auditory Research, University College London, London, UK.

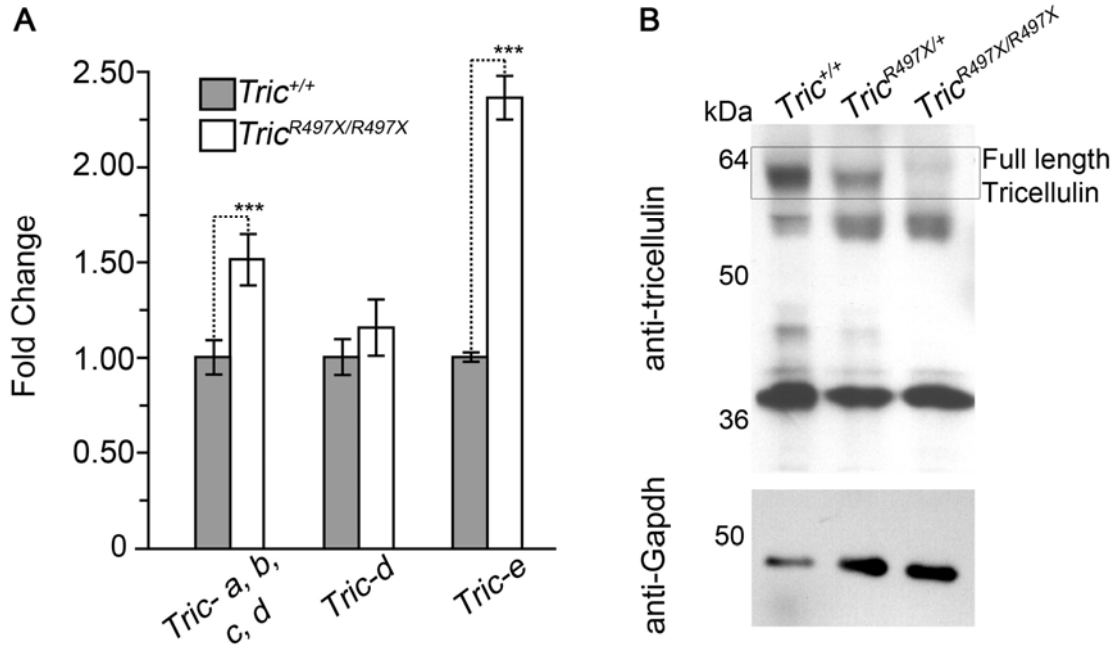

Supplemental Figure 1

Alternate transcripts of Tric are overexpressed in Tric$^{R497X/R497X}$ mice. (**A**) Real time Taqman assays to quantitate the various *Tric* isoforms in the inner ear cDNA of P10 *Tric$^{+/+}$* and *Tric$^{R497X/R497X}$* mice. Shown above are the relative fold changes in the *Tric$^{R497X/R497X}$* samples (open bars) compared to the controls (grey bars). (mean ± 95% confidence interval). n=5 mice/genotype. Statistically significant overexpression was seen for *Tric-a* to *c* isoforms combined, as well as for *Tric-e* (***, P<0.001). (**B**) Western blotting of inner ear protein lysates from P8 *Tric$^{+/+}$* and *Tric$^{R497X/R497X}$* mice. The tricellulin bands corresponding to the full length protein (~64 kDa) are enclosed within the box. Our results show lack of full-length tricellulin protein in *Tric$^{R497X/R497X}$* inner ear lysates as compared to control samples. Additional protein products seen in the *Tric$^{+/+}$, Tric$^{R497X/+}$* and *Tric$^{R497X/R497X}$* inner ear lysates may reflect the lower molecular weight tricellulin isoforms (Figure 1E) (24).

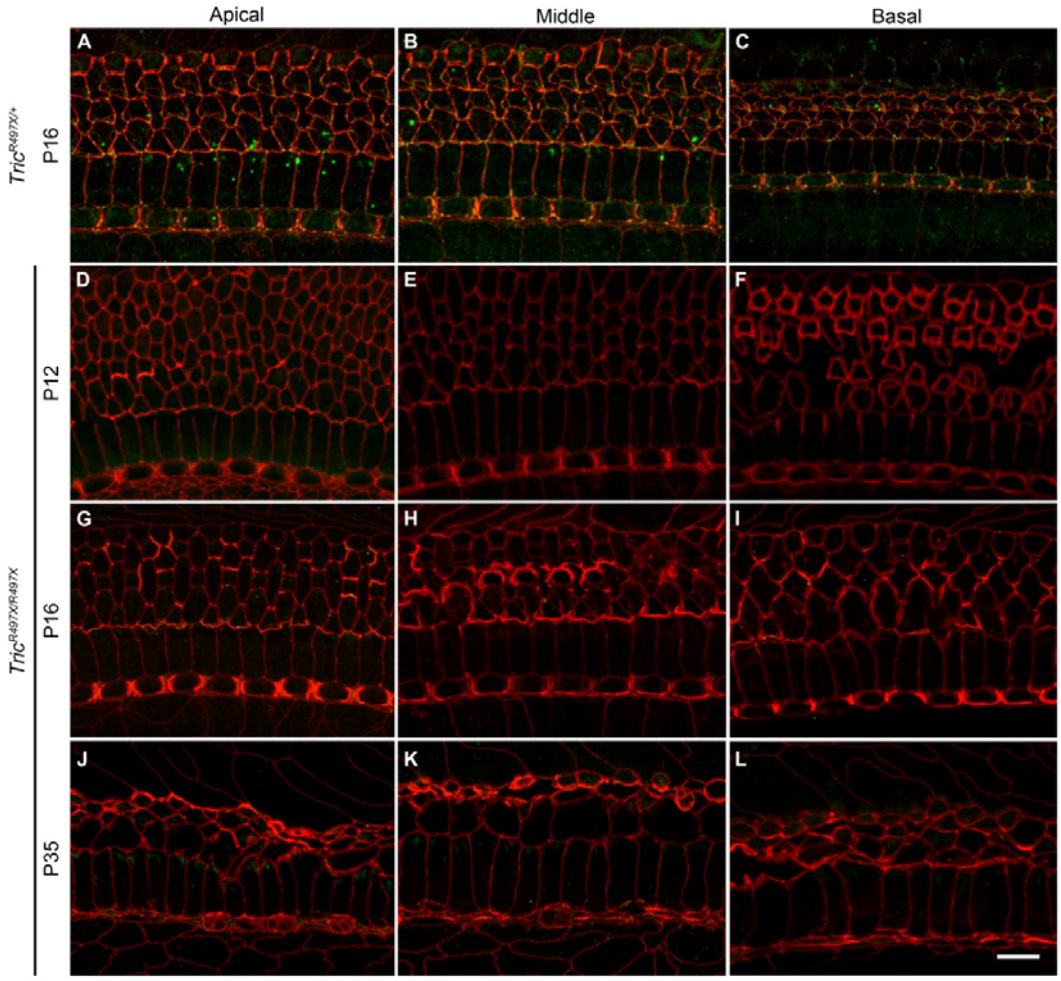

Supplemental Figure 2

Tricellulin is absent from the tight junctions in the organ of Corti of Tric$^{R497X/R497X}$ mice. Maximum projections of confocal Z-stacks of cochlear whole-mounts co-labeled with the tricellulin antibody, PB705, (green) and ZO1 (red). (**A-C**) Immunohistochemistry of the whole mount organ of Corti from the three turns of the cochleae of *Tric*$^{R497X/+}$ control mice at P16. (**D-L**) Images of the organ of Corti from the three turns of the cochleae of P12 (**D-F**), P16 (**G-I**) and P35 (**J-L**) *Tric*$^{R497X/R497X}$ mice. The tricellulin antibody labels the tricellular junctions in the organ of Corti of control mice but the labeling is lost in the *Tric*$^{R497X/R497X}$ mice. The hair cell degeneration pattern is similar to that shown in Figure 3 and Supplemental Figure 3. Scale bar applies to all panels and represents 10 µm.

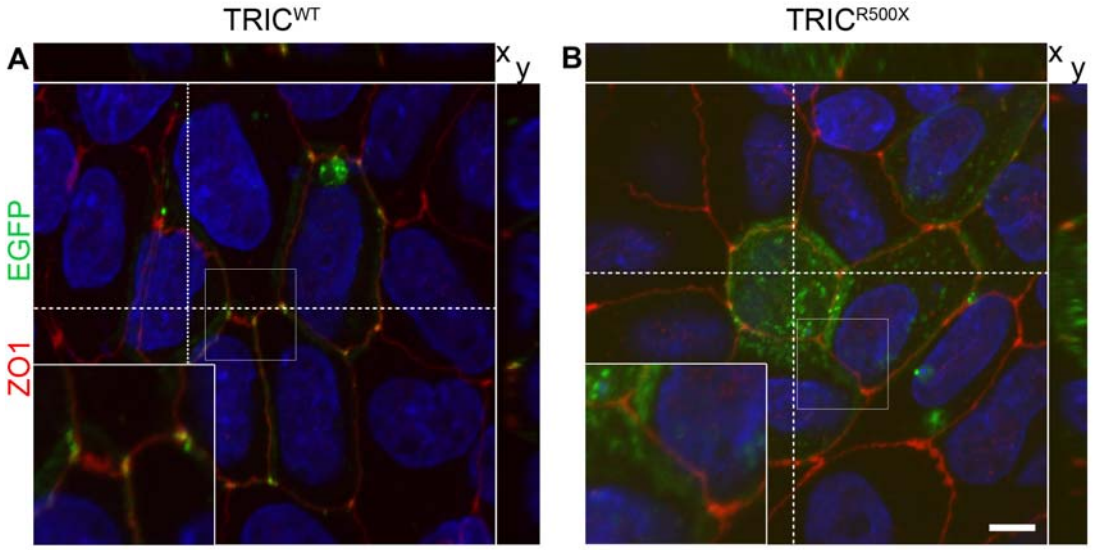

Supplemental Figure 3

The p.Arg500 mutation results in loss of the tricellular junction targeting signal*. The images are orthogonal Z projections of MDCKII cells expressing wild-type TRIC and TRIC^{R500X}. (**A**) MDCK cells expressing wild-type human tricellulin TRIC^{WT} (green) and labeled with a ZO1 antibody (red).Orthogonal sections through the tricellular and bicellular junctions (x and y axis) show that the protein was enriched at tricellular junctions but also localized weakly to the bicellular tight junctions. (**B**) MDCK cells expressing TRIC^{R500X} (green) and labeled with a ZO1 antibody (red). Orthogonal sections through the tricellular and bicellular junctions (x and y axis) show that TRIC^{R500X} was no longer enriched at the tricellular junctions but was still found at the bicellular junctions and basolateral plasma membrane. In both panels, the insets show a magnified view of the tricellular tight junctions enclosed by the small boxes. Blue is DAPI. Scale bar, 5 µm.

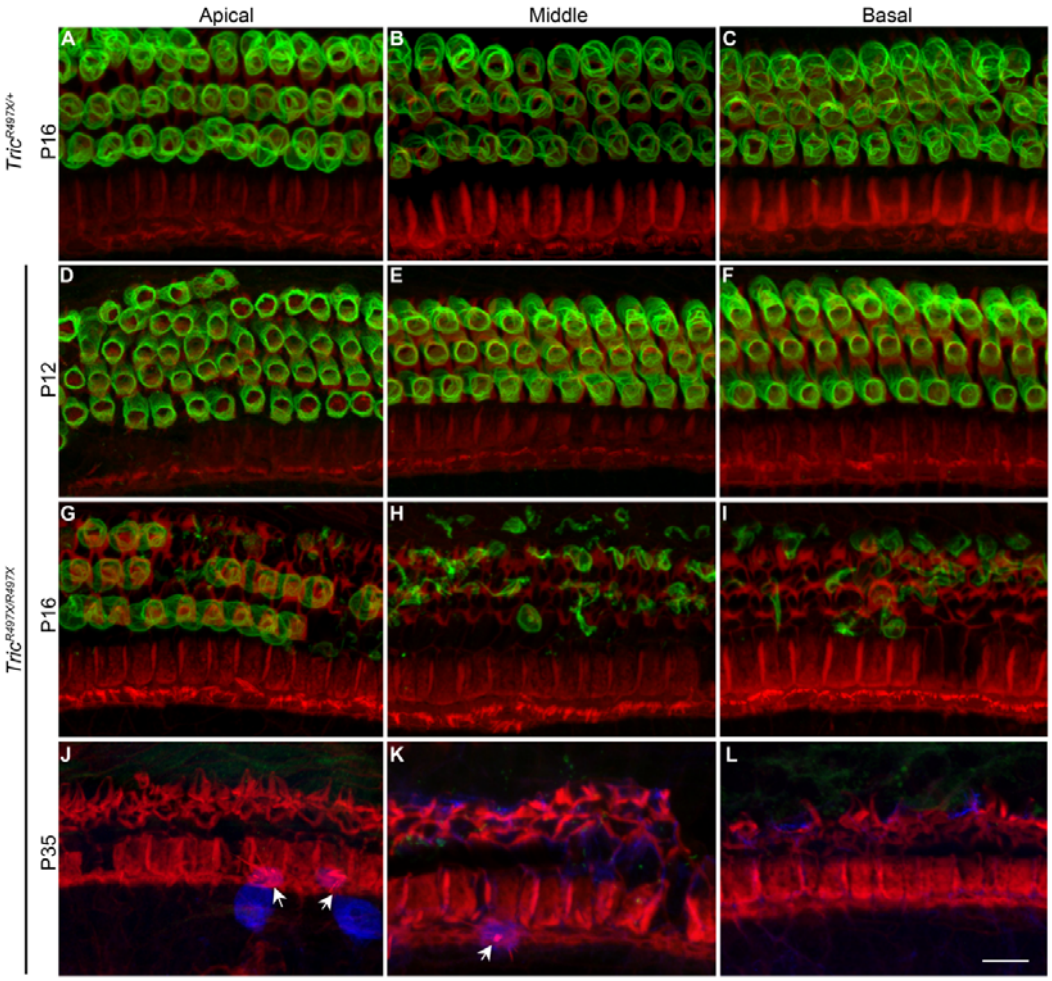

Supplemental Figure 4

Outer hair cells in the Tric$^{R497X/R497X}$ mice undergo rapid degeneration in the third and fourth weeks of life. Shown here are maximum projections of confocal Z-stacks of cochlear whole-mounts labeled with prestin antibody (green), a unique protein expressed in OHCs, and counter-stained with phalloidin labeling of cytoskeletal, filamentous actin (red). (**A-C**) Representative images from the apical, middle and basal turns of the organ of Corti of *Tric$^{R497X/+}$* (control) mouse at P16. (**D-L**) Images of the organ of Corti from the three turns of the cochlea of *Tric$^{R497X/R497X}$* mice at P12 (**D-F**), P16 (**G-I**) and P35 (**J-L**). While the hair cells appear to have normal development and morphology at P12 in the knock-in mice, severe outer hair cell degeneration can be seen by P16. The OHC loss progresses rapidly, followed by

inner hair cell loss. By P35, only few IHCs remain in the apical and middle turns of the cochlea. These IHCs, identified through additional labeling by calretinin in blue (arrows), have abnormal stereocilia as revealed by rhodamine-phalloidin staining (arrows). Scale bar is in panel **L** is 10 µm and applies to all panels.

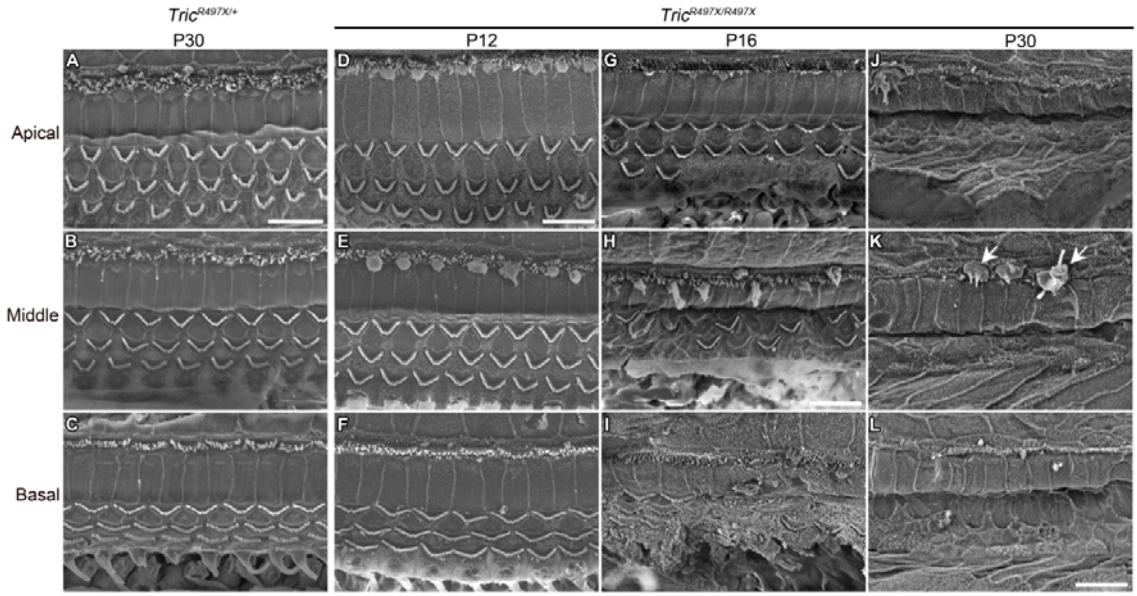

Supplemental Figure 5

Absence of tricellulin leads to loss of cochlear hair cells. (**A-C**) show the normal surface morphology of the organ of Corti of the three cochlear turns of P30 *Tric* $^{R497X/+}$ mice. (**D-L**) Surface morphology of similar regions of the cochlea of P12 (**D-F**), P16 (**G-I**) and P30 (**J**-**L**) *Tric*$^{R497X/R497X}$ mice. The surface of the reticular lamina of cochleae from *Tric*$^{R497X/R497X}$ mice appears normal at P12 but degeneration of OHCs can be seen by P16. The degeneration is more severe at the basal end than the apical end at this age. By P30 however, all hair cells along the length of the cochlea are degenerated except for a few abnormal looking IHCs. All OHCs are replaced by supporting cells. All scale bars are 10 µm and the scale bar in **A** applies to **B**, **C**, **E**, **F**, **G** and **I-K**.

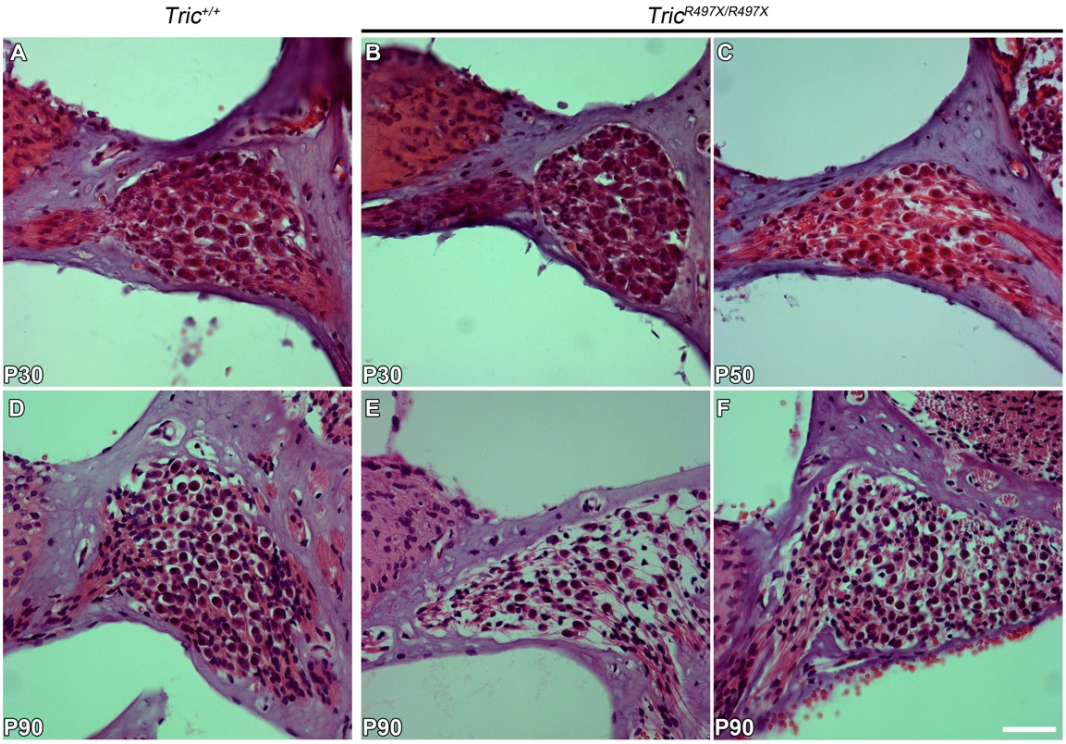

Supplemental Figure 6

The spiral ganglion neurons of Tric$^{R497X/R497X}$ mice progressively degenerate.

Hematoxylin and eosin labeling of cryosections of inner ears from *Tric*$^{+/+}$ (**A, D**) and *Tric*$^{R497X/R497X}$ mice (**B**, **C**, **E** and **F**) from various developmental time points. All panels show the basal turns of the cochleae. No significant degeneration was observed at P30 (**B**) and P50 (**C**) in *Tric*$^{R497X/R497X}$ mice. However, at P90 obvious loss of spiral ganglion neurons was observed in *Tric*$^{R497X/R497X}$ mice (**E**, **F**) as compared to age-matched littermate control mice (**D**). Scale bar is 25 µm.

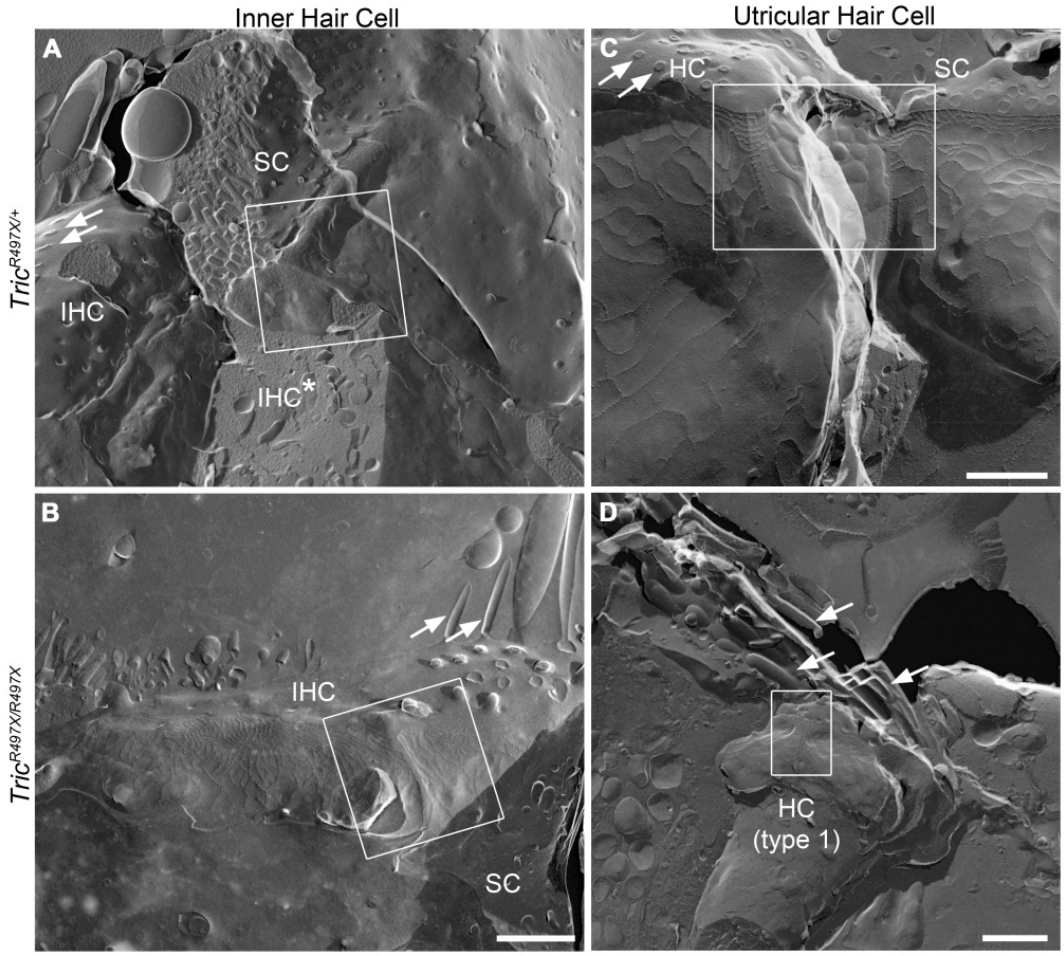

Supplemental Figure 7

Tricellulin is required for the normal development of the tricellular junction structure. (**A-D**) Low power electron microscopy images of freeze-fracture replica of tricellular tight junctions shown in Figure 5C-G. (**A**) Tricellular junction (box) shown in Figure 5C. The supporting cell (SC) and the cross-fractured inner hair cells (IHC*) that relate to the junction are indicated. A third supporting cell is “fractured away” providing an en face view of the tricellular junction. Another IHC that is adjacent to the SC is also indicated and small arrows point to the profiles of cross-fractured stereocilia across the apical surface. (**B**) Tricellular junction (box) in Figure 5D. The IHC and SC that relate to this junction are shown and the arrows indicate the stereocilia bundles at the apical surface of the IHC. (**C)** Two tricellular junctions (box)

shown in Figure 5E. The tricellular junction to the left is formed by the HC contacting two supporting cells that were removed during fracturing. Small arrows indicate cross-fractures of stereocilia at the apical surface of the HC. The tricellular contact to the right is formed by a central supporting cell contacting the SC and the HC. (**D**) Tricellular junction (box) shown in Figure 5F. The two supporting cells that the HC would have contacted at this junction have been fractured away. Arrows point to stereocilia bundle at the apical surface of the HC. Scale bar in **B** is 1 µm and applies also to **A**. Scale bar in **C** is 0.5 µm and **D** is 1 µm.

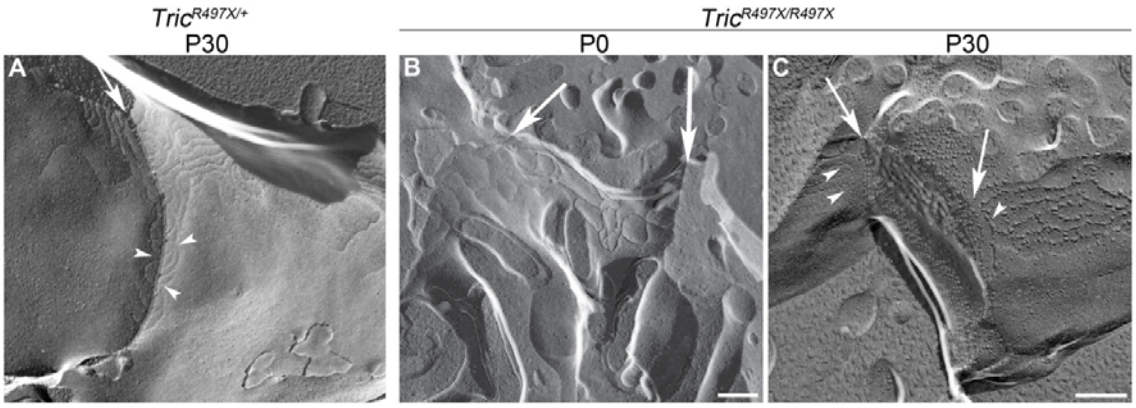

Supplemental Figure 8

Loss of tricellulin results in alterations in the ultrastructure of the tricellular tight junctions in the marginal cell layer of the stria vascularis. (**A-C**) Freeze fracture replica electron microscopy images of tricellular tight junctions of stria vascularis marginal cells of *Tric*$^{R497X/+}$ mice at P30 (**A**) and *Tric*$^{R497X/R497X}$ mice at P0 (**B**) and P30 (**C**). (**A**) At P30, the tricellular tight junctions in the *Tric*$^{R497X/+}$ mice are well defined and the elements of the bicellular junctions are seen converging at the tricellular junction (arrowheads). (**B**) In the P0 *Tric*$^{R497X/R497X}$ mice, there is an absence of the “fishbone”-like structures of the tricellular junction (arrows). (**C**) In the P30 *Tric*$^{R497X/R497X}$ mice, although the tricellular tight junctions look more developed compared to that seen in the P0 mutant, they seem to be formed of disconnected particles (**C**, arrows). Also, the elements of the bicellular junction do not converge at the tricellular junction but unite with each other (**C**, arrowheads). Scale bars 200 nm. Scale bar in B applies also to A.

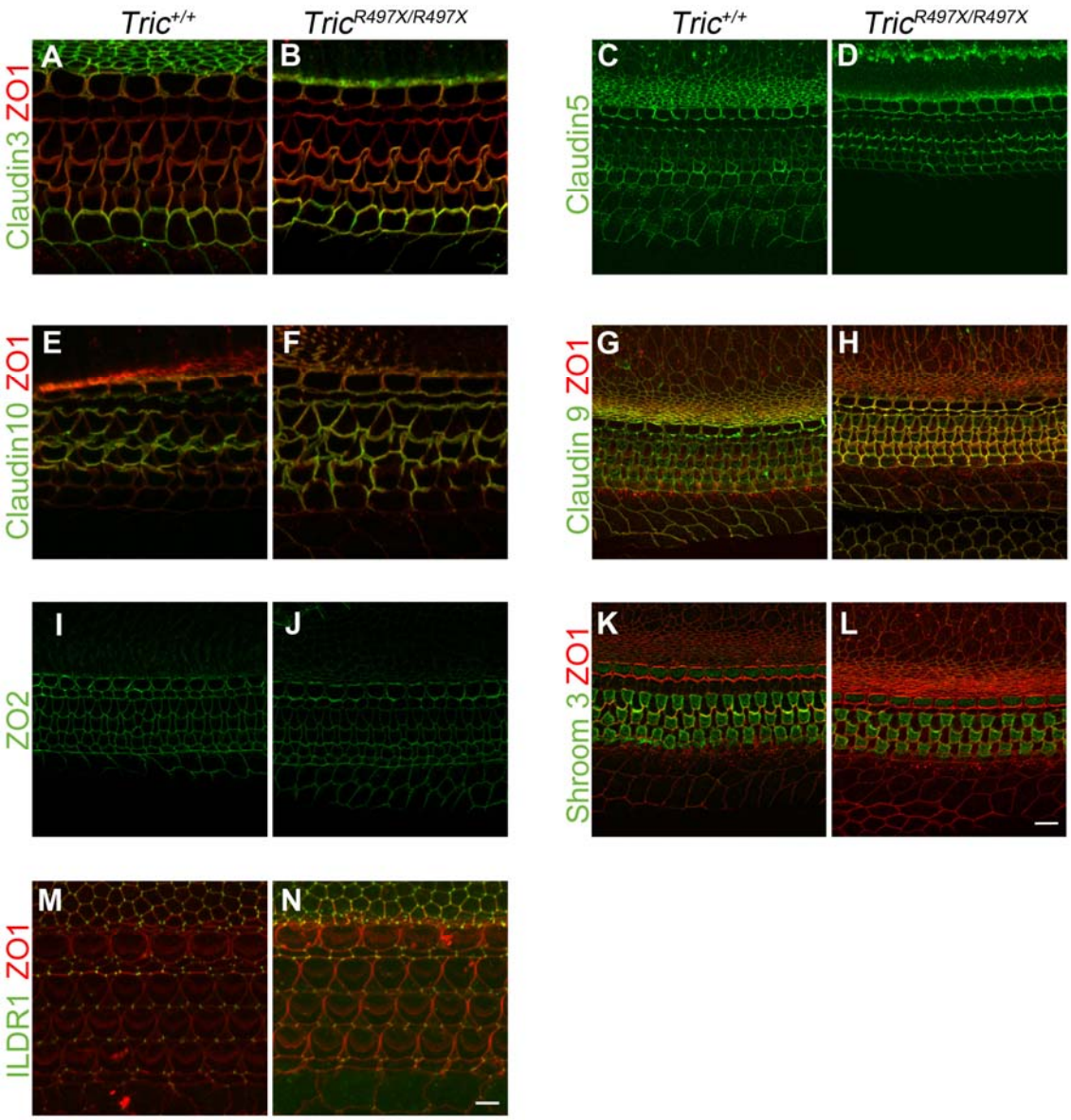

Supplemental Figure 9

Localization of other tight junction proteins is not altered in the organ of Corti of *Tric*$^{R497X/R497X}$ *mice.* (**A-B**) Immunolocalization of claudin 3 in the organ of Corti of P10 *Tric*$^{+/+}$ (**A**) and *Tric*$^{R497X/R497X}$ (**B**) mice. (**C-D**) Immunolocalization of claudin 5 in the organ of Corti of P9 *Tric*$^{+/+}$ (**C**) and *Tric*$^{R497X/R497X}$ (**D**) mice. (**E-F**) Immunolocalization of claudin 10 in the organ of Corti of P10 *Tric*$^{+/+}$ (**E**) and *Tric*$^{R497X/R497X}$ (**F**) mice. (**G-H**) Immunolocalization of claudin 9 in the organ of Corti of

P10 *Tric*$^{+/+}$ (**G**) and *Tric*$^{R497X/R497X}$ (**H**) mice. (**I-J**) Immunolocalization of ZO2 in the organ of Corti of P9 *Tric*$^{+/+}$ (**I**) and *Tric*$^{R497X/R497X}$ (**J**) mice. (**K-L**) Immunolocalization of shroom3 in the organ of Corti of P10 *Tric*$^{+/+}$ (**K**) and *Tric*$^{R497X/R497X}$ (**L**) mice. (**M-N**) Immunolocalization of ILDR1 in the organ of Corti from the basal region of P2 *Tric*$^{+/+}$ (**M**) and *Tric*$^{R497X/R497X}$ (**N**) mice cochleae. The red channel in all panels refers to ZO1 labeling. Scale bar in **N** is 5 µm and applies also to **A**, **B**, **E** and **F**. Scale bar in **L** is 10 µm and applies also to **C**, **D**, **G-K**).

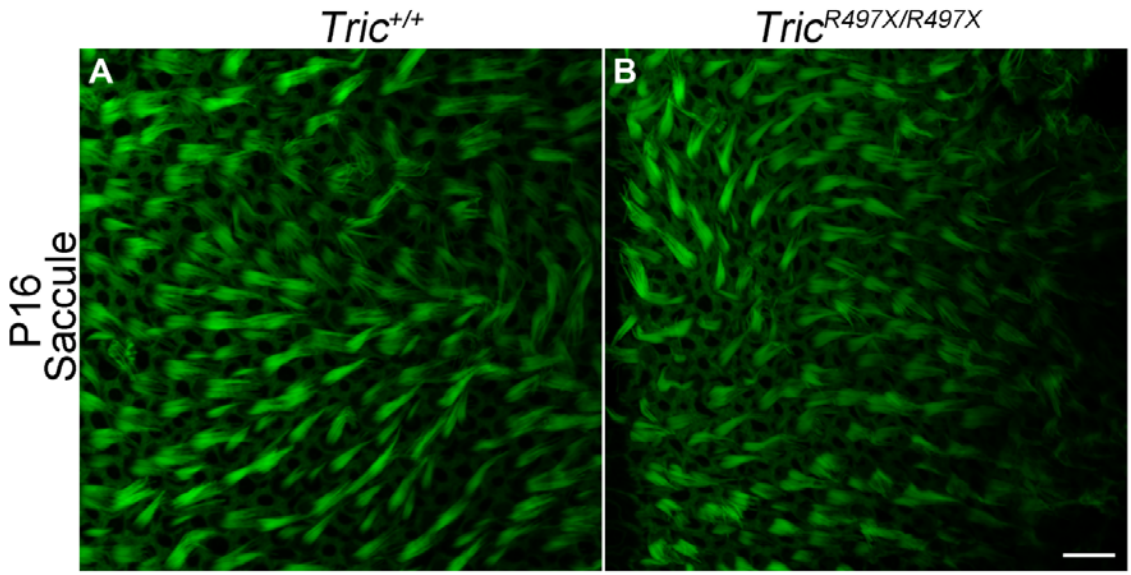

Supplemental Figure 10

There is no hair cell degeneration in the vestibular organs of the tricellulin knock-in mice. Confocal images of phalloidin-labeled whole mounts of saccule of *Tric*$^{+/+}$ (**A**) and *Tric*$^{R497X/R497X}$ littermates (**B**) at P16. Scale bar is 10 µm.

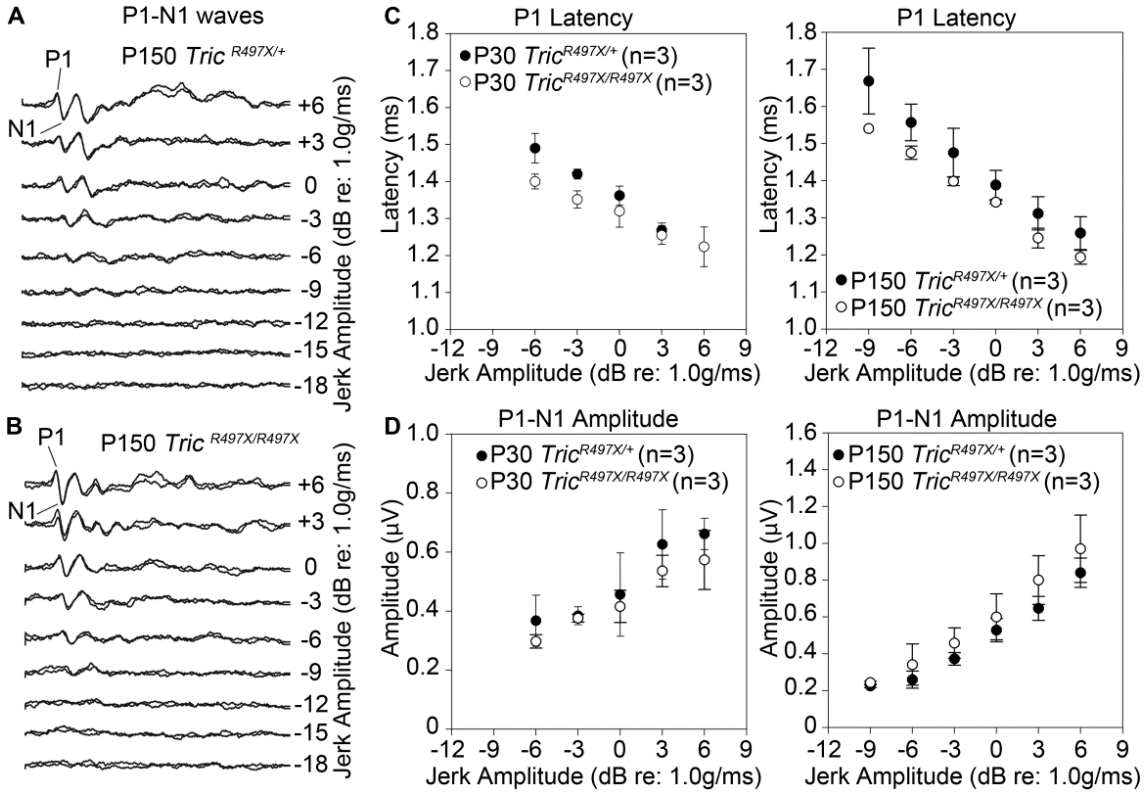

Supplemental Figure 11

Vestibular function is unaffected in Tric$^{R497X/R497X}$ mice. (**A** and **B**) Representative vestibular evoked potential waveforms generated in response to linear jerk stimuli in *Tric$^{R497X/+}$ and Tric$^{R497X/R497X}$* mice, respectively, at P30. Both groups of mice showed similar robust responses indicated by the P1 and N1 peaks (**C**). The P1 latencies (mean ± SEM; n=3/genotype) and (**D**) the P1-N1 amplitudes of *Tric$^{R497X/+}$* (filled circles) and *Tric$^{R497X/R497X}$* (open circles) mice were identical at P30 (left panels) and P150 (right panels).

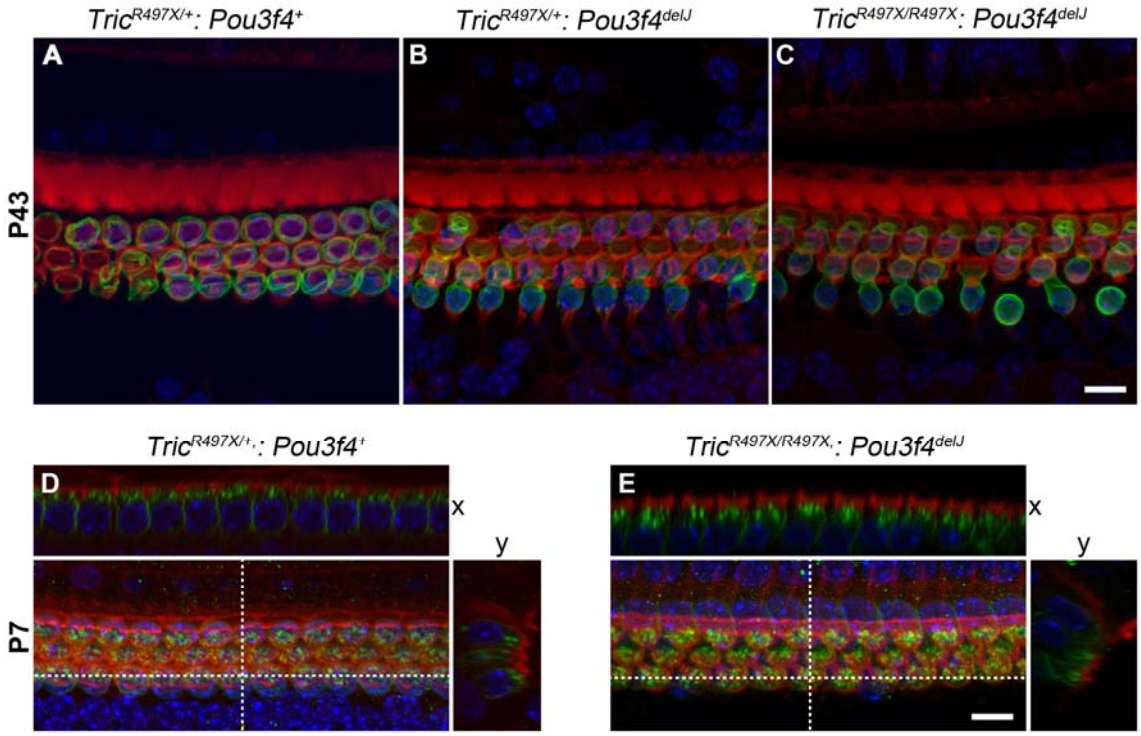

Supplemental Figure 12

Hair cell degeneration is rescued in older Tric$^{R497X/R497X}$: Pou3f4^{delJ} mice. (**A-C**) Confocal images of prestin antibody (green) and phalloidin (red) labeled cochlear sensory epithelia of *Tric$^{R497X/+}$: Pou3f4^{+}* (**A**), *Tric$^{R497X/+}$: Pou3f4^{delJ}* (**B**) and *Tric$^{R497X/R497X}$: Pou3f4^{delJ}* mice (**C**) at P43. (**D** and **E**) Maximum projections and corresponding orthogonal sections through confocal stacks of the organ of Corti of *Tric$^{R497X/+}$: Pou3f4^{+}* mice (**D**) and *Tric$^{R497X/R497X}$: Pou3f4^{delJ}* mice (**E**) at P7. The samples were immunolabeled with prestin antibody (36). There were no observable differences in the localization of prestin in the OHCs of *Tric$^{R497X/+}$: Pou3f4^{+}* and *Tric$^{R497X/R497X}$: Pou3f4^{delJ}* mice. Scale bar in **C** is 5 µm and applies also to **A** and **B**. Scale bar in **E** is 5 µm and applies also to **D**.

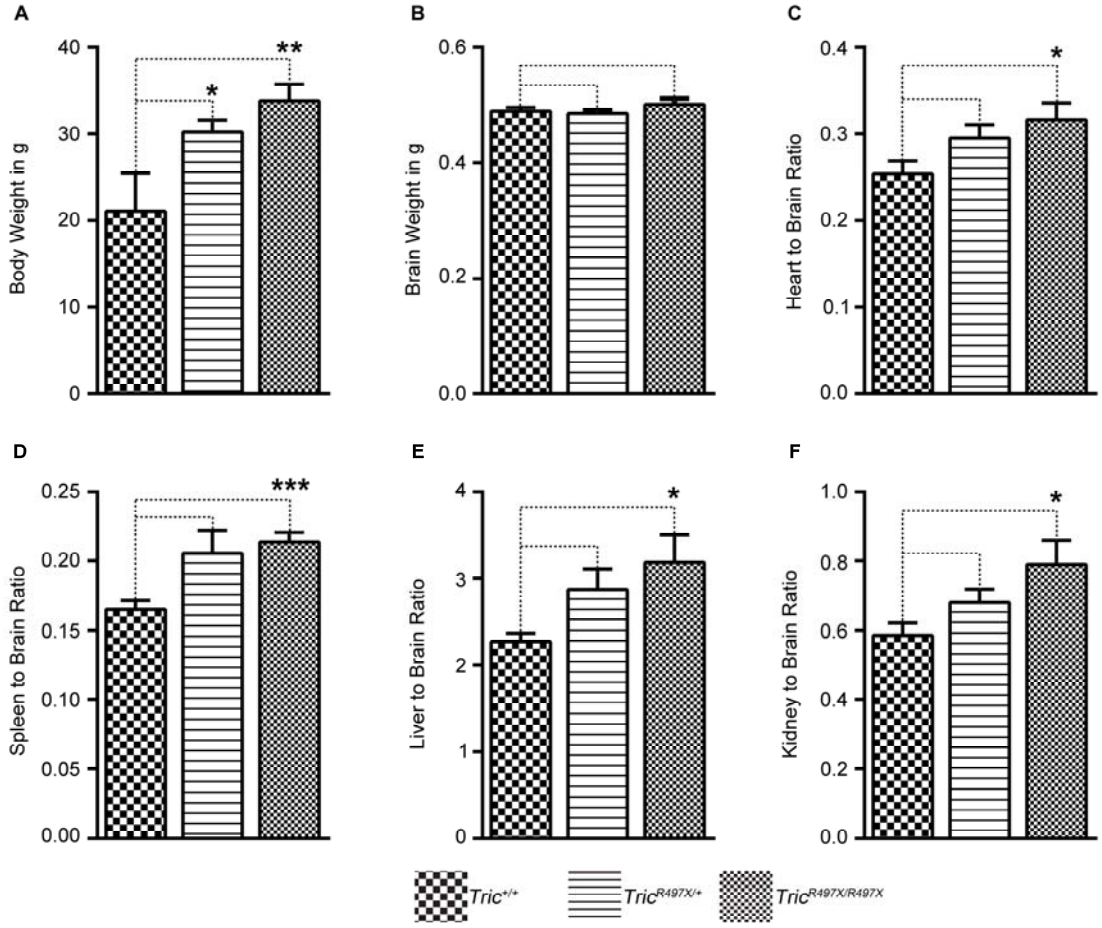

Supplemental Figure 13

p.Arg497 mutation results in phenotypic changes in body and organ weights.*

Shown are the phenotypic changes seen in 3 month old *Tric*$^{R497X/+}$ and *Tric*$^{R497X/R497X}$ mice compared to the *Tric*$^{+/+}$ mice. The body and organ weights of mice of all three genotypes are plotted along with the mean and standard deviation. (**A**) Body weights of *Tric*$^{R497X/+}$ and *Tric*$^{R497X/R497X}$ mice were significantly higher than those of *Tric*$^{+/+}$ mice although (**B**) brain weights were the same between the genotypes. (**C**) The heart to brain ratio was significantly higher in the *Tric*$^{R497X/R497X}$ mice, as was the (**D**) spleen to brain ratio, (**E**) liver to brain ratio and (**F**) kidney to brain ratio.(mean ± SEM; n=5 for *Tric*$^{+/+}$, n=6 for *Tric*$^{R497X/+}$ and *Tric*$^{R497X/R497X}$ mice) **P*<0.05; ***P*<0.01; ****P*<0.001.

Supplemental Table 1. List of genotyping, RT-PCR and real time Taqman primers.

Primers	**Reaction**	**Sequence**
Forward primer for *Tric* p.Arg497* allele	Genotyping	CGAGAACGCTATAAGGCTGTG
Reverse primer for *Tric* p.Arg497* allele	Genotyping	ACCATACCCGAGACCTGAGTT
Tric-F	RT-PCR	GTGAAAATCACAAATGTCGTCAAGT
Tric-R	RT-PCR	AGAACCTTAAACTATCCCAGCTGAA
Primer and probe set *Tric-a, b, c* and *d* isoforms	Real Time Taqman assay	F AATGACTCCTGAGCTGTTGAGTGG Probe ATCGTGATGCCTGACTACGTGGCAAA R TCCGCAGACAGCTCTTTGTACTCT
Primer and probe set for *Tric- d* isoform	Real Time Taqman assay	F TAAAGCTGTGGAGGCACGAAGC Probe AGTTCCTGGAGCAGCAGGAGTGTGAA R TTCCTGATCCCTCTGTCGATCACT
Primer and probe set for *Tric-e* isoform	Real Time Taqman assay	F ACATTCCGAAGCCTATCGTG Probe TGCCTGACTACGTGGCGAACA R TCTTTTTCCTAAACTCTTCATGAATTCT
Primer and probe set for Gapdh	Real time Taqman assay	F GTG GAG TCA TAC TGG AAC ATG TAG Probe TGC AAA TGG CAG CCC TGG TG R AAT GGT GAA GGT CGG TGT G

Supplemental Table 2. Results of serum chemistry analysis of *Tric*$^{+/+}$, *Tric*$^{R497X/+}$ and *Tric*$^{R497X/R497X}$ mice.

Serum Chemistry	**Normal range**	**Units**	***Tric*$^{+/+}$ ***	***Tric*$^{R497X/+}$ ****	***Tric*$^{R497X/R497X}$ ****
Glucose	115.3 - 323.27	mg/dL	235.8	225.33	230.33
Cholesterol	51.72 - 171.11	mg/dL	86	92.83	90.83
Triglycerides	5.52 - 228.34	mg/dL	62	91.33	105.17
Blood urea nitrogen	13.5 - 37.47	mg/dL	20.8	23.83	29.33
Creatinine	0.1-0.2	mg/dL	0.19	0.18	0.22
Total protein	4.2 - 5.8	g/dL	4.88	5.48	5.08
Albumin	2.39 - 3.56	g/dL	2.78	3.02	2.72
Alanine aminotransferase	13 - 108.56	U/L	24	29	33.67
Aspartate aminotransferase	31 - 224.38	U/L	79.6	59.83	55.33
Alkaline phosphatase	6 - 251.1	U/L	95.8	72	63.5
Total bilirubin	0.02 - 0.77	mg/dL	0.22	0.23	0.22
Calcium	7.62 - 9.73	mg/dL	8.92	8.58	9.42
Inorganic phosphorous	4.07 - 11.25	mg/dL	6.1	7.1	7.42
Creatine kinase	35-200	U/L	218.2	57.83	144.67
Lactate dehydrogenase	54 - 657.56	U/L	218.4	154	157.5

Average Values of 5 (*) and 6 (**) mice

Supplemental Table 3. Results of hematological analysis of *Tric*$^{+/+}$, *Tric*$^{R497X/+}$ and *Tric*$^{R497X/R497X}$ mice.

Hematology	**Normal Range**	**Units**	***Tric*$^{+/+}$ ***	***Tric*$^{R497X/+}$ ****	***Tric*$^{R497X/R497X}$ ****
White blood cells count	0.6 - 6.38	x10^3/µl	4.1	3.266667	4.28
Neutrophil absolute count	0.001 - 2.52	x10^3/µl	0.698	0.73	0.948333
Lymphocyte absolute count	0.36 - 4.46	x10^3/µl	3.262	2.38	3.143333
Monocyte absolute count	0.01 - 0.52	x10^3/µl	0.118	0.146667	0.165
Eosinophil absolute count	0 - 0.12	x10^3/µl	0.02	0.008333	0.018333
Basophil absolute count	0 - 0.04	x10^3/µl	0.004	0	0.003333
Red blood cell count	7.7 - 10.13	x10^6/µl	9.654	9.326667	9.136667
Hemoglobin	12.29 - 15.53	g/dL	14.5	14.21667	13.85
Hematocrit	36.78 - 49.13	%	47.84	48.21667	46.21667
Platelet count	532 - 1300	x10^3/µl	662.2	586.3333	692.1667
Mean corpuscular volume	43.6 - 53.27	fL	49.54	51.58333	50.53333
Mean corpuscular hemoglobin	15.35 - 15.97	pg	15.02	15.23333	15.15
Mean corpuscular hemoglobin concentration	31.5 - 33.4	g/dL	30.4	29.61667	30.08333

Average Values of 5 (*) and 6 (**) mice